Low Temperature X-ray Diffraction Study of ZnCr2O4 and Ni0.5Zn0.5Cr2O4

メタデータ	言語: eng 出版者: 公開日: 2017-10-03 キーワード (Ja): キーワード (En): 作成者: メールアドレス: 所属:
URL	http://hdl.handle.net/2297/9546

Low Temperature X-ray Diffraction Study of $ZnCr_2O_4$ and $Ni_{0.5}Zn_{0.5}Cr_2O_4$

Yun Xue, Shumsun Naher, Fumiaki Hata , Hiroshi Kaneko, Haruhiko Suzuki and Yoshihiro Kino*

Department of Physics, Faculty of Science, Kanazawa University

Kakuma-machi, Kanazawa 920-1192, Japan

*X-ray Laboratory, Rigaku Corporation, 3-9-12, Matsubara-cho, Akishima-shi, Tokyo 196, Japan

Results of x-ray diffraction measurements are presented for $ZnCr_2O_4$ and $Ni_{0.5}Zn_{0.5}Cr_2O_4$. Splits of the x-ray diffraction spectrum are observed in $ZnCr_2O_4$ at 12 K. In $Ni_{0.5}Zn_{0.5}Cr_2O_4$ no clear split is observed, but a full width at half maximum (*FWHM*) shows a steep increase below about 20 K. It is found that the integrated intensity of the diffraction spectra shows a softening behavior at low temperatures in $ZnCr_2O_4$.

1. INTRODUCTION

Geometrical frustration is one of the most interesting topics in the study of condensed matter systems. Frustrated interactions often cause extensive degeneracy in the ground state of the system and prevent any ordering down to low temperatures. The ground state of a frustrated system at absolute zero temperature is quite intriguing, and can be modified into a novel and interesting state, associated with quantum fluctuations. The degenerated states, however, remove its degeneracy in general by a broken symmetry, such as a crystal distortion at low temperatures. Whether geometrically frustrated systems undergo the crystal distortion or are modified into a new state without a crystal distortion is a very interesting subject. Among these geometrically frustrated systems

there are triangular lattices, kagome structure, pyrochlore compounds and spinel compounds. We have already suggested the occurrence of the crystal distortion in a spin-ice state of pyrochlore compounds such as $Dy_2Ti_2O_7$ and $Ho_2Ti_2O_7$ below the spin-ice temperature [1]. We examined a crystal distortion of a spinel compound $ZnCr_2O_4$, using low temperature x-ray diffraction. $ZnCr_2O_4$ has a cubic structure with a space group $Fd\bar{3}m$ in the paramagnetic state at high temperature. Non-magnetic Zn^{2+} and magnetic Cr^{3+} ions have a strong preference for the tetrahedral A- and the octahedral B-sites, respectively. The B-sites in the spinel structure form a network of tetrahedra sharing their corners with four neighbors. Consequently, magnetic spins on the B-sites are geometrically frustrated with respect to the antiferromagnetic interaction between the nearest neighbors. The frustration suppresses the long-range magnetic order. The sound velocity for the $(c_{11}- c_{12})/2$ mode shows a considerable softening as it approaches T_N, antiferromagnetic transition temperature. This is evidence that the magnetic phase transition is accompanied by a structural transition [2-3]. Therefore, $T_c(T_N)<<|\Theta_{CW}|$ stands, here Θ_{CW} is the asymptotic Curie temperature. Θ_{CW} = -388 K was obtained from the magnetic susceptibility measurement [4]. Elastic and inelastic neutron

measurements revealed that $ZnCr_2O_4$ undergoes a first order phase transition at 12.5 K into a tetragonal phase with Néel order [5]. From these results of neutron experiments, Lee et al. discussed a new spin state above the phase transition temperature, that is, a new spin cluster state of six tetrahedra which can be realized in the geometrically frustrated system associated with quantum fluctuation [6]. They also discussed the phase transition at 12.5 K as a spin-Peierls-like phase transition.

X-ray powder diffraction was performed in the temperature range from 100 K and 4.3 K by Kagomiya et al. [7]. The refinement of the observed spectrum below T_N was performed by the Rietveld analysis method, assuming tetragonal ($I4_1/amd$) or orthorhombic ($Fddd$) symmetry. They obtained better fitting for the $Fddd$ symmetry than for the $I4_1/amd$ symmetry. A Cr^{3+} ion is not a so-called Jahn-Teller ion, that is, the ground state of Cr^{3+} has no orbital degeneracy. $ZnCr_2O_4$ distorts to break the symmetry of the degenerated frustrated spin states by the spin-Peierls-like phase transition. On the other hand, $NiCr_2O_4$ undergoes a Jahn-Teller phase transition from a cubic phase to a tetragonal phase with $c > a$, at a temperature of 310 K, differing from the low temperature magnetic transition temperature T_N [8]. The Nickel-Zinc-Chromite system

($Ni_xZn_{1-x}Cr_2O_4$) has been studied for x=0, 0.37, 0.67, 0.73 and 1 by elastic constants and thermal expansion measurements [9]. It was found that for $x > 0.6$, this system exhibits a cooperative Jahn-Teller phase transition which occurs at a temperature T_c higher than the magnetic phase transition at T_N. For x=0 and 0.37, the structure and magnetic transitions occur at the same temperature; that is, the magnetic transition, spin-Peierls-like transition induces the crystal distortion. In our present paper $Ni_{0.5}Zn_{0.5}Cr_2O_4$ was also investigated, which had not previously been studied. The magnetic phase transition and Jahn-Teller crystal phase transition are believed to occur at temperatures which are very close to each other. This might be an example of the system in which the magnetic interaction and the Jahn-Teller interaction are in competition with each other. This is also interesting system from the point of view of quantum fluctuation. Two different interactions, which are competed with each other, enhance the quantum fluctuation.

In the present paper x-ray diffraction experiments were carried out through the phase transition at 12 K for $ZnCr_2O_4$. Temperature variations of lattice constants, full width at half maximum (*FWHM*) and integrated intensity of the x-ray diffraction spectrum were

measured in detail. Especially in the vicinity of the transition temperature, measurements were performed while changing the temperature by 0.2 K per step as shown in Fig. 3.

2. EXPERIMENTS

Two different types of cooling systems were used in our low temperature x-ray diffraction experiments depending on the temperature range. Above about 10 K, a ^{4}He circulating cryocooler was used and below 10 K, a ^{3}He-^{4}He dilution refrigerator (D.R.). A D.R. itself reaches 20 mK, but with an x-ray beam, the lowest temperature in our experiment was about 120 mK which achieved the thermal equilibrium of the specimen. X-ray diffraction measurements for powder specimens were performed using the RINT 2500 system, Rigaku Co.. An x-ray beam was generated by a rotating Cu anode. At several temperatures entire profiles of reflection peaks were measured with a step size of 0.01° and a step-counting time of 6 s. For some reflection planes x-ray diffraction measurements with a step size of 0.005° and a step-counting time of 60 s were performed to accumulate more counts at certain temperatures. From the observed profile the lattice constant *d*, the integrated intensity (*I. I.*) and also the *FWHM* were obtained.

In these analyses the profile was fitted to a Pseude-Voight function.

3. RESULTS and DISCUSSION

3.1 $ZnCr_2O_4$

At several temperatures whole profiles of reflection peaks were measured and refined by the Rietveld method using the reported crystal structure. The observed X-ray diffraction profiles at 300 K and 1.7 K with the Rietveld refinements using "RIETAN-2000"[10] are shown in Fig. 1a and Fig.1b. As shown, the refinement is rather good. Refinement precision is given by the value of S = 2.076 for 300 K profile. A lattice constant of the cubic structure was obtained to be a= b= c= 8.71079 Å at 300 K. At 1.7 K, the profile well fits the tetragonal (*I41/amd*). Lattice constants of the tetragonal structure were obtained as $2^{1/2}a = 2^{1/2}b$ = 8.33697 Å and c = 8.32011 Å. Refinement precision is S = 1.5274 for the 1.7 K profile. Profiles of $\theta - 2\theta$ scans of (800) Bragg reflection of the cubic unit cell of $ZnCr_2O_4$ at 20 K ($T > T_c$) and at 0.2 K ($T < T_c$) are shown in Fig.2a and 2b. In these figures the Cu $K\alpha_2$ spectra are subtracted from the observed reflection spectra by calculations using the Rachinger method. From

these results, it is also confirmed that the symmetry of $ZnCr_2O_4$ lowers into tetragonal below T_c. Below T_c the profile of (800) Bragg reflection split into two peaks, the lower angle peak having twice the intensity of the higher peak. From this result it is found that the tetragonal *c*-axis is shorter than the tetragonal *a'*-axis which we define as $2^{1/2}a$ ($= 2^{1/2}b$). The value of *c/a'* at 0.2 K was 0.998 which is rather good coincidence with the value obtained from the Rietveld analysis. Profiles of $\theta - 2\theta$ scans of (400) Bragg reflections were measured in the vicinity of the phase transition temperature. Between 12.8 K and 10.8 K profiles measured at every 0.2 K step are shown in Fig. 3. The horizontal axis represents the rotation 2θ angle from 42° to 44.5°, and the vertical axis shows the diffraction reflective intensity. These profiles contain Cu $K\alpha_2$ spectra. The smaller peak existing in the right shoulder of the peak is due to the reflection of the K_β line. Based on the results the temperature dependences of the lattice constants obtained for the (400) reflection are shown in Fig. 4 around the transition temperature, and from the figure it is found that the transition temperature of our specimen is 12 K. The temperature dependence of the crystal distortion in $ZnCr_2O_4$ suggests the first order phase transition. The *I.I.* also suggests the phase transition even though the scattering of

the data is rather large. The integrated intensity of the x-ray diffraction spectra can be expressed using the Debye-Waller factor,

$$I = I_0 \mathrm{ecp}(-1/3 < u^2 > \sin^2\theta_B) \qquad (1)$$

where I_0 is the scattered intensity from the rigid lattice and θ_B is the scattering angle. Here, $< u^2 >$ is the mean square displacement of the atom. At high temperatures where the thermal average $1/2M\omega^2 < u^2 >$ of a classical harmonic oscillator in three dimension can be given by $3/2k_BT$, the diffraction intensity is

$$I = I_0 exp(-k_B T \sin^2\theta_B / M\omega^2) \qquad (2)$$

where M is the mass of the atom and ω is the frequency of the oscillator.

At low temperatures the displacement of atom, u is caused by a recoil-free fraction of absorption and emission of photons by atoms in crystals, which is similar to the Mössbauer effect. The recoil-free energy can be expressed by $E_R = 1/2M(h/\lambda_o)^2$ where h is the Planck's constant and λ_0, the wavelength of x-rays. In the case of the Cu target we used, λ_0 is 0.15406 nm. Using E_R, the diffraction intensity is given by the equation,

$$I = I_0 exp(-2E_R \sin^2\theta_B / 3M\omega^2) \ . \qquad (3)$$

The temperature dependence of the *I.I.* of (400) reflection is shown in Fig. 5. When the

thermal effect is dominant in the Debye-Waller effect the *I.I.* should increase with decreasing temperature following equation 2. The *I.I.* of (400) reflection shown in Fig. 5, however, decreases with decreasing temperature, suggesting the softening of the lattice, that is, the phonon frequency ω in equation 3 is becoming smaller with decreasing temperature. In the inset of Fig. 5 the *I.I.* in the vicinity of the transition temperature is shown in the expanded scale. The *I.I.* also shows a clear change at the phase transition temperature. In Fig. 6 the *I.I.* of (311) reflection is plotted against temperature. In a high temperature region above 100 K, the *I.I.* increases with decreasing temperature. Below about 100 K the *I.I.* begins to decrease until about 30 K and then again increases below 30 K. These results suggest the anisotropic Debye-Waller factors. We will not discuss these factors further here, however, these results also suggest the softening of the lattice. The sound velocity $v = (c_{44}/\rho)^{1/2}$ measured by Kino and Lüthi also shows the softening of the lattice down to about 50 K and then the sound velocity increases with decreasing temperature. They also measured the sound velocity $v = (c_{11}\text{-}c_{12}/2\rho)^{1/2}$, which shows the softening down to the transition temperature. The transition temperature of their specimen was 9.5 K[2].

3.2 $Ni_{0.5}Zn_{0.5}Cr_2O_4$

The magnetic susceptibility of $Ni_{0.5}Zn_{0.5}Cr_2O_4$ crystal was measured between 1.8 K and 300 K by a SQUID magnetometer MPS system produced by QUANTUM Design Co., Ltd.. The inverse of magnetic susceptibility is plotted against temperature in Fig. 7 while the magnetic susceptibility vs. temperature is shown in the inset of that figure. The temperature dependence of the magnetic susceptibility is very different from that of $ZnCr_2O_4$. The magnetic susceptibility of $ZnCr_2O_4$ shows the broad maximum and then sharp drop at the transition temperature. As shown in Fig. 7, the magnetic susceptibility of $Ni_{0.5}Zn_{0.5}Cr_2O_4$ does not show the broad maximum, but shows rather sharp peak at 16.5 K. Above 120 K the magnetic susceptibility is expressed by a Curie-Weiss relation $\chi = C/(T - \Theta_{CW})$ with the asymptotic Curie temperature Θ_{CW} = -498 K, larger antiferromagnetic interaction than the value of Θ_{CW} = -388 K of $ZnCr_2O_4$. The temperature of the maximum of magnetic susceptibility, 16.5 K, is also higher than the magnetic transition temperature T_N = 12 K in $ZnCr_2O_4$.

By x-ray diffraction a clear split of the diffraction spectrum due to the crystal distortion was not observed, though the crystal phase transition temperature is higher than one in

$ZnCr_2O_4$. This can be explained as following; $NiCr_2O_4$ shows a Jahn-Teller distortion from cubic to tetragonal with $c > a$, while $ZnCr_2O_4$ is distorted below T_N with $c < a$. Therefore, the resulting distortion in the mixed system of $Ni_{0.5}Zn_{0.5}Cr_2O_4$ must be rather small compared to the pure system.

In Fig. 8, a *FWHM* of (440) reflection is plotted against temperature. The *FWHM* starts to increase at about 20 K with decreasing temperature, suggesting the occurrence of the crystal distortion. At the lowest temperature of 10 K it is not yet saturated, in contradiction to the sharp transition in $ZnCr_2O_4$. The same temperature dependence of *FWHM* was also observed for the (800) reflection, not shown here. This broadness of the phase transition can again be explained by the competition of two different interactions and also by the fact that both magnetic and crystal phase transitions occur at close temperatures. When we define the antiferromagnetic transition as the maximum of the magnetic susceptibility shown in Fig. 7, it is 16.5 K in our measurements. When the antiferromagnetic transition is defined at the temperature where $d\chi/dT$ value takes the maximum, T_N would be slightly lower than 16.5 K. The crystal phase transition must be at about 20 K. The temperature dependence of the integrated intensity is shown in Fig.9

for (440) reflection. An expanded low temperature portion is shown in the inset of the figure. It shows the softening down to about 200 K and then the I.I. increases slowly. Below about 20 K, the integrated intensity increases drastically till about 16 K. Unfortunately no sound velocity measurement has been reported for $Ni_{0.5}Zn_{0.5}Cr_2O_4$. However, for other concentration compounds, such as $Ni_{0.67}Zn_{0.33}Cr_2O_4$ the sound velocity for shear mode $v = (c_{44}/\rho)^{1/2}$ shows the softening down to about 80 K with decreasing temperature and then decreases slightly down to the T_N of 14 K. Below T_N it increases so steep.

4. CONCLUSION

In this paper we studied $ZnCr_2O_4$ and $Ni_{0.5}Zn_{0.5}Cr_2O_4$ using x-ray diffraction measurements. We observed a clear split of the x-ray diffraction spectrum in $ZnCr_2O_4$ at 12 K, from which we could deduce the value of c/a =0.998 < 1. But we could not observe the spectrum split in $Ni_{0.5}Zn_{0.5}Cr_2O_4$. This might be because the magnetic transition by Cr^{3+} ion with c/a < 1 and the crystal phase transition by Ni^{3+} ion with c/a > 1 occur at temperatures very close to each other. However, the *FWHM* clearly shows the

phase transition below about 20 K, though we were unable to distinguish the magnetic transition which is about 16.5 K from our susceptibility measurement and the crystal phase transition.

The integrated intensity of the (400) reflections in $ZnCr_2O_4$ shows the softening behavior. The softening was also observed in the sound velocity by Kino and Lüthi [2]. In $Ni_{0.5}Zn_{0.5}Cr_2O_4$ the I.I. also decreases down to about 200 K. Unfortunately no sound velocity measurement has been reported for $Ni_{0.5}Zn_{0.5}Cr_2O_4$. But sound velocity of $Ni_{0.67}Zn_{0.33}Cr_2O_4$ shows the softening down to about 80 K.

The magnetic properties of $Ni_{0.5}Zn_{0.5}Cr_2O_4$ below T_N and also above T_N are very interested in. Though the magnetic ground state of $ZnCr_2O_4$ is not yet determined.

REFERENCES

1. H. Suzuki, F. Hata, Y. Xue, H. Kaneko, A. Hosomichi, S. Abe, R. Higashinaka, S. Nakatsuji and Y. Maeno, *AIP Conf. Proc*. **850** 1109 (2006)
2. Y. Kino and B. Lüthi, *Solid State Commun*. **9** 805 (1971).
3. R. Plumier, M. Lecomte and M. Sougi, *J. Phys. (Paris)* **38** L149 (1977).
4. H. Martino, N. O. Moreno, J. A. Sanjujo, C. Rettori, A. J. Garcia-Adeva, D. L. Huber, S. B. Oseroff, W. Ratcliff II, S, -W. Cheong, P. G. Pagliuso, J. L. Sarrao and G. B. Martins, *J. Appl. Phys*. **89** 7050 (2001).
5. S.-H. Lee, C. Broholm, T. H. Kim, W. Ratcliff and A.-W. Cheong, *Phys. Rev. Lett*. **84** 3718 (2000).
6. S.-H. Lee, C. Broholm, W. Ratcliff, G. Gasparovic, G. Husang, T. H. Kim and S. –W. Cheong, *Nature* **418** 856 (2002).

7. I. Kagomiya, H. Sawa, K. Siratori, K. Kohn, M. Toki, Y. Hata and E. Kita, *Ferroelectrics*, **268** 327 (2002).
8. Y. Kino and S. Miyahara, *J. Phys. Soc. Jpn.* **20** 1522 (1965).
9. Y. Kino, B. Lüthi and M. E. Mullen, *J. Phys. Soc. Jpn.* **33** 687 (1972).
10. F. Izumi and T. Ikeda, *Mater. Sci. Forum*, **321-324** 198 (2000)

FIGURE CAPTIONS

Fig. 1a. Observed (closed circle), calculated (solid line) and difference profiles from Rietveld analysis of the $ZnCr_2O_4$ sample at room temperature. Inset shows (311) reflection in expanded scale.

. 1b. Profiles from Rietveld analysis of $ZnCr_2O_4$ sample at 1.7 K. Notations are the same as in Fig. 1. Inset shows (311) reflection in expanded scale.

Fig. 2a. Profile of θ - 2θ scans of (800) Bragg reflection of the cubic unit cell of $ZnCr_2O_4$ at 20 K ($T > T_c$).

. 2b. Profile of θ - 2θ scans of (800) Bragg reflection of the cubic unit cell of $ZnCr_2O_4$ at 0.2 K ($T < T_c$).

Fig. 3. Profile of θ - 2θ scans of (400) Bragg reflection of the cubic unit cell of $ZnCr_2O_4$ in the vicinity of the transition temperature. The profiles contain the $CuK\alpha_2$ reflections. Intensity of each profiles above 11.0 K are shifted by 500 counts.

Fig. 4. Temperature dependence of the lattice constants obtained from the (400) reflection in $ZnCr_2O_4$. a is the lattice constant of the cubic structure and a'($=2^{1/2}a=2^{1/2}b$) and c are lattice constants of the tetragonal structure.

Fig. 5. Temperature dependence of the *I.I.* of (400) reflection in $ZnCr_2O_4$. Inset shows low temperature portion in expanded scale.

Fig. 6. Temperature dependence of the *I.I.* of (311) reflection in $ZnCr_2O_4$.

Fig. 7. Inverse of the magnetic susceptibility vs. temperature. Straight line expresses Curie-Weiss approximation $\chi^{-1} = C/(T - \theta_{cw})$ with = -488 K. Inset shows magnetic susceptibility of $Ni_{0.5}Zn_{0.5}Cr_2O_4$ vs. temperature.

Fig. 8. *FWHM* of (440) reflection in $Ni_{0.5}Zn_{0.5}Cr_2O_4$ vs. temperature.

Fig. 9. Integrated intensity of (440) reflection in $Ni_{0.5}Zn_{0.5}Cr_2O_4$ vs. temperature. Inset shows low temperature portion of the figure in expanded scale.

Figures

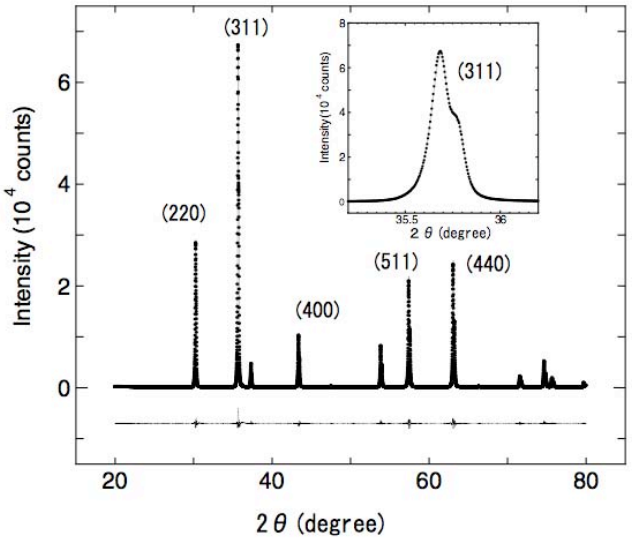

Fig. 1a.

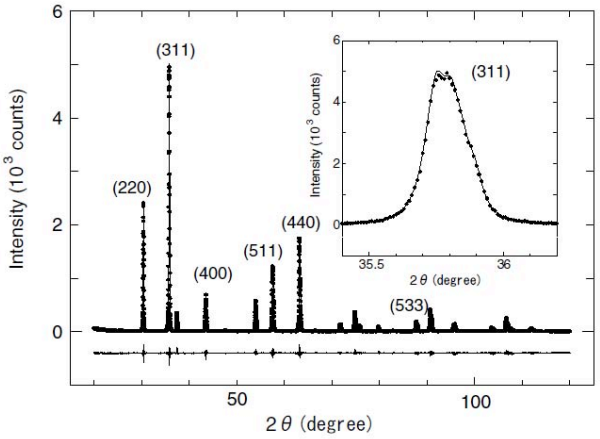

Fig. 1b.

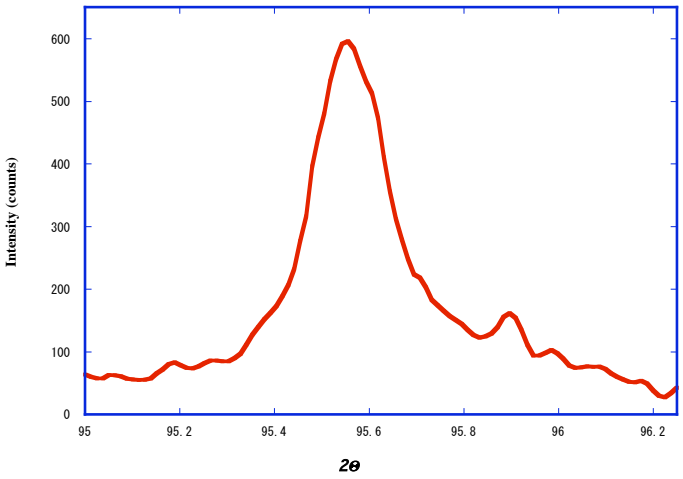
Intensity (counts)
600
500
400
300
200
100
0
95
95. 2
95. 4
95. 6
95. 8
96
96. 2
2θ

Fig. 2a.

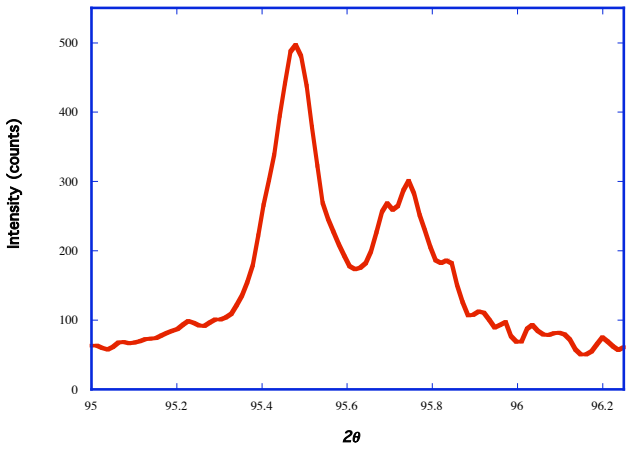
Intensity (counts)
500
400
300
200
100
0
95
95.2
95.4
95.6
95.8
96
96.2
2θ

Fig. 2b.

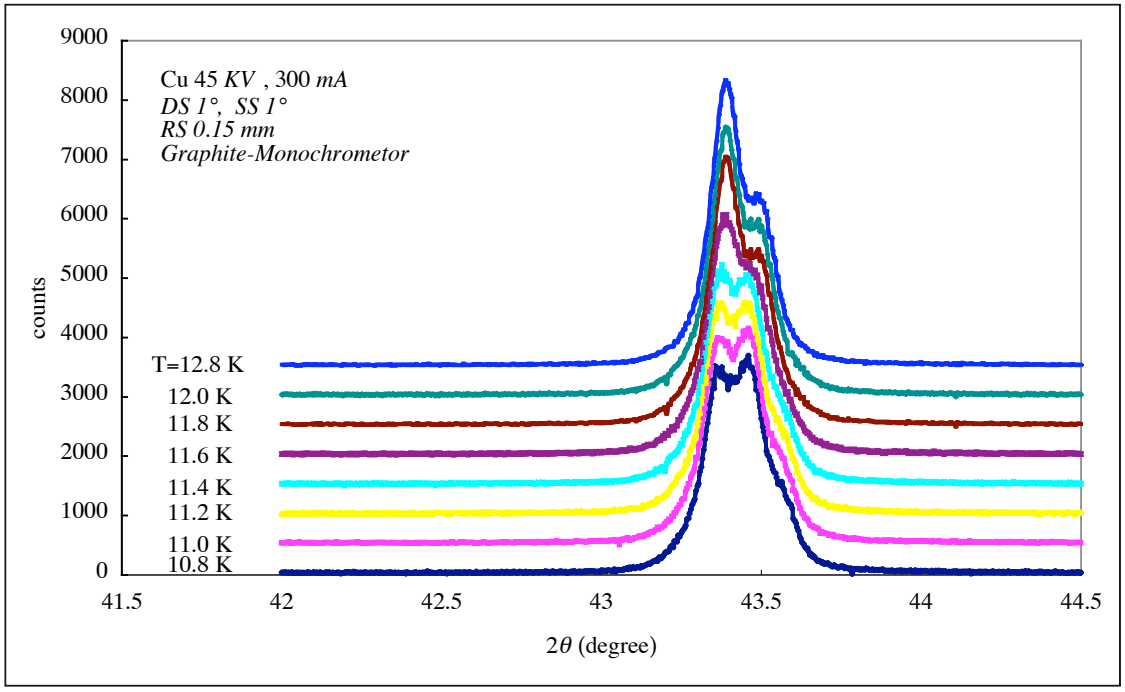
Cu 45 KV , 300 mA
DS 1°, SS 1°
RS 0.15 mm
Graphite-Monochrometor
counts
T=12.8 K
12.0 K
11.8 K
11.6 K
11.4 K
11.2 K
11.0 K
10.8 K
2θ (degree)

Fig. 3.

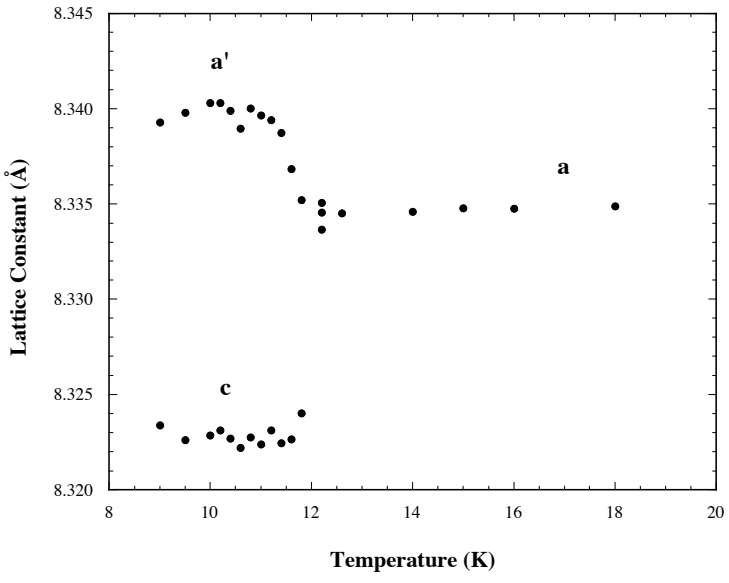
a'
a
c
Lattice Constant (Å)
Temperature (K)

Fig. 4.

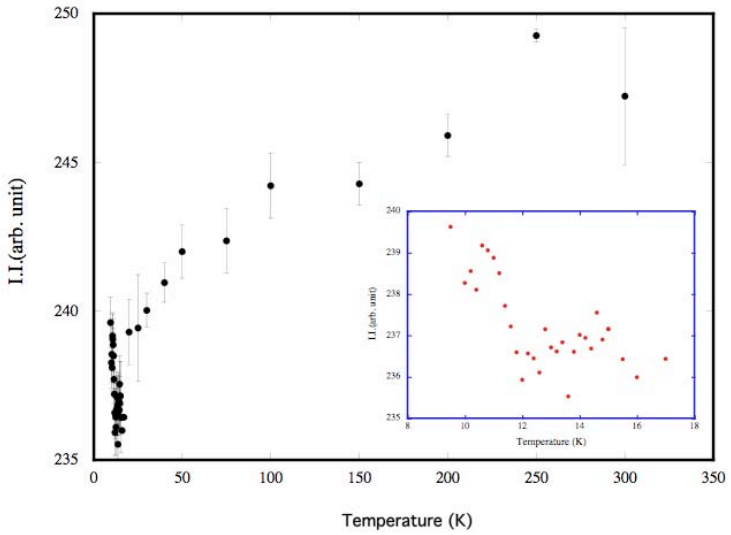
I.I.(arb. unit)
Temperature (K)
250
245
240
235
0
50
100
150
200
250
300
350
240
239
238
237
236
235
8
10
12
14
16
18
I.I.(arb. unit)
Temperature (K)

Fig. 5.

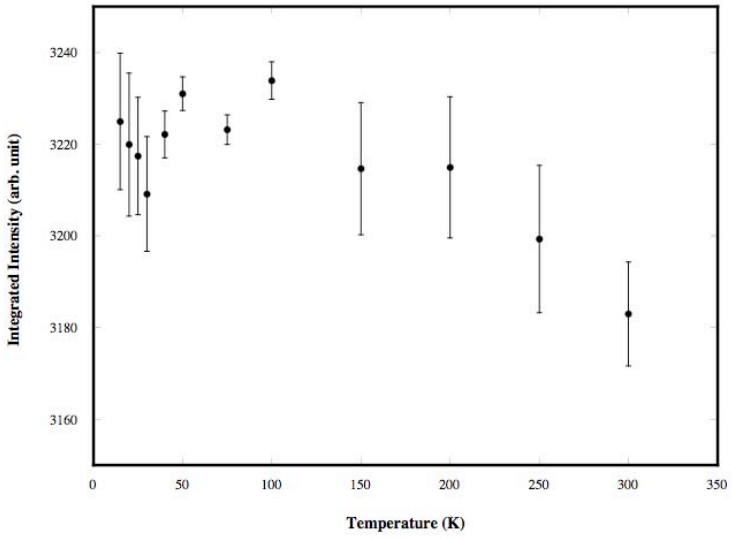
Integrated Intensity (arb. unit)
Temperature (K)
3240
3220
3200
3180
3160
0
50
100
150
200
250
300
350

Fig. 6.

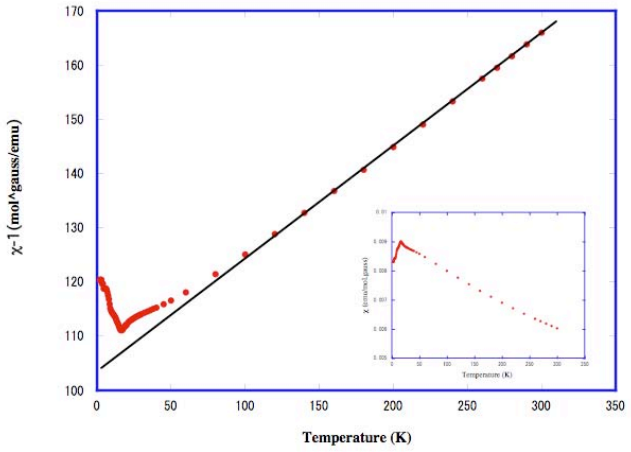
χ^-1 (mol^gauss/emu)
Temperature (K)

Fig. 7.

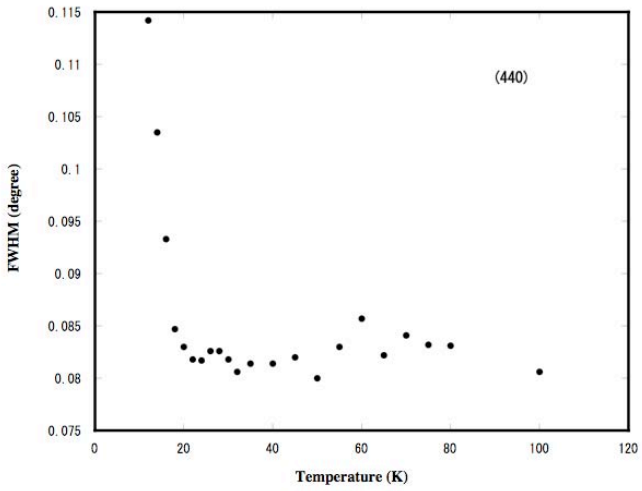
(440)
FWHM (degree)
Temperature (K)

Fig. 8.

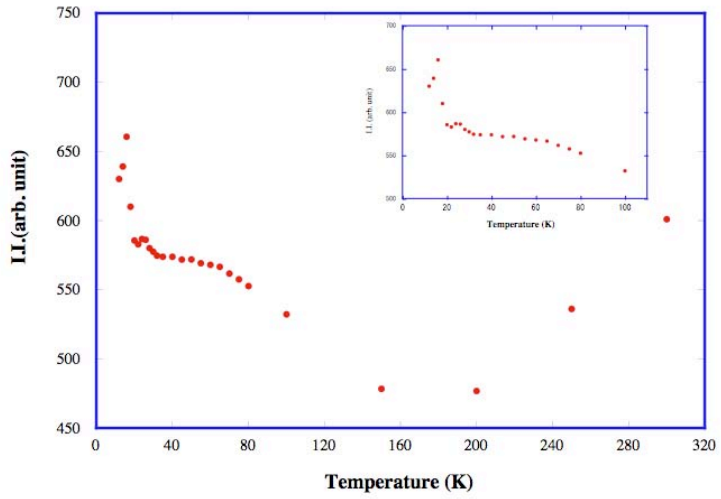
I.I.(arb. unit)
Temperature (K)
750
700
650
600
550
500
450
0
40
80
120
160
200
240
280
320

Fig. 9.